Visualisation of the Local Electrochemical Activity of Thermally-Sprayed Anti-Corrosion Coatings using Scanning Electrochemical Microscopy

Darren A. Walsh,* Lisa Li, Bakare Mayowa,[†] K. T. Voisey[†]

School of Chemistry, The University of Nottingham, Nottingham NG7 2RD, UK

[†] Faculty of Engineering, The University of Nottingham, Nottingham NG7 2RD, UK

*Corresponding Author**:**

darren.walsh@nottingham.ac.uk

Tel: +44 115 951 3437 Fax: +44 115 951 3562

ABSTRACT

Scanning electrochemical microscopy was used to probe the local electrochemical activity of anti-corrosion coatings formed from Inconel 625, a Ni-Cr-Mo alloy commonly used in engineering applications. The coatings were formed using a high velocity oxygen fuel thermal spraying technique. Upon spraying onto mild steel substrates, clear splat boundaries were formed at the interface between droplets of the alloy as they cooled on the substrate surface. Scanning electrochemical microscopy in the feedback mode, employing ferrocenemethanol as redox mediator, was used to determine the local electrochemical activity of samples of the wrought alloy, the sintered alloy and the thermally-sprayed coating. Significantly, the wrought and sintered materials generally showed responses typical of those expected for a purely insulating material. However, feedback approach curve data showed that the electrochemical activity of the entire thermally-sprayed coating was higher than that of the bulk alloy. Local variations in the coating's activity were then visualised using scanning electrochemical microscopy. These observations indicate that the spraying process increases the conductivity of Inconel 625 and that localised regions of increased electrochemical activity are generated throughout the material, which appear to be related to the splat boundaries formed during spraying.

Keywords: corrosion; thermal-spray; alloys; high velocity oxygen fuel; scanning electrochemical microscopy

2

1.   Introduction

The corrosion resistance of inexpensive materials can be significantly enhanced by modifying the surface with thermally-sprayed anti-corrosion coatings [1].   The obvious advantage of this process is the significant cost reduction compared to using bulk alloys. The introduction of high velocity oxygen fuel (HVOF) processes was a highly-important development in thermal-spray technology, significantly improving the quality of the coatings [2,3]. Significantly-reduced deposition times, increased densities and reduced porosities can be achieved using HVOF processing techniques. Research in this area currently includes the development of nanostructured coatings prepared using HVOF processes, which can exhibit enhanced physical and mechanical properties [4,5]. There is also considerable current activity regarding the use of HVOF cermet coatings as a replacement for hard chrome [6] and characterisation of the mechanical properties and corrosion behaviour of HVOF coatings [7,8].

The HVOF process involves using a supersonic jet to propel the feedstock powder through an expansion nozzle. The jet accelerates and heats the particles, partially melting them. On impacting the substrate the particles deform, spread out and adhere primarily by mechanical interlocking. The coating is built up from the impacts of successive particles producing a distinctive lamellar microstructure. Compared to other thermal-spray processes, such as plasma spraying, HVOF is a higher-velocity, lower temperature technique. Consequently, the coating particles impact the substrate surface at a much higher speed than is encountered in typical flame spray processes.   Overall, HVOF coatings can exhibit significantly improved characteristics and performances compared to those formed using more traditional spray-coating technologies. However, optimum corrosion resistance can only be achieved if the spray parameters and powder type and composition are optimised.

Therefore, considerable work is being undertaken to investigate the effects of such parameters on the performance of the resultant coatings [9,10,11,12]. Despite this effort, process-inherent inclusions and pores can remain within the coatings and may have a detrimental effect on the corrosion resistance. Previous work has identified a performance gap between the corrosion resistance of thermally-sprayed coatings and the corresponding bulk alloys [13]. This performance gap is attributed to the distinct differences in microstructure of the bulk and sprayed material. The details of the links between microstructural features and corrosion performance are not fully understood. However, it has been shown that the performance gap is not simply due to interconnected porosity limiting the effectiveness of the coating as a barrier to corrosion [14,15].

Inconel alloys are Ni-based alloys that are used in extreme environments due to their high strength and stability at extreme temperatures. Inconel 625 is particularly useful in applications such as gas turbines and the aerospace industry due to high processability [16,17]. It also shows some excellent anti-corrosion properties and is therefore a very promising coating for the protection of less-expensive materials. The passivating oxide layer that forms on the surface of Inconel 625 is a layered structure with an inner layer of Cr-Ni oxide and an outer Mo-Cr oxide layer [18]. Various literature reports exist that describe the corrosion resistance behaviour of Inconel 625 coatings, which is usually studied using potentiostatic or potentiodynamic analysis of the coated surface [19,20]. However, despite the work that has been devoted to the microstructural properties and electrochemical properties of Inconel coatings [14,15], comparatively little is understood regarding the development of pitting sites and the role of microstructural features in product failure. High-resolution electron microscopy is often combined with bulk electrochemical analysis and correlation between the two analyses is difficult.

Scanning electrochemical microscopy (SECM) is a very useful technique for characterizing local electrochemical activity and pitting at films. Significantly, the inclusions and pores commonly found on HVOF thermal-sprayed coating are tens of microns in diameter, which is an ideal feature size for SECM analysis [21]. SECM has been used previously by others to study the corrosion properties of surfaces. For example, the local reactivity of titanium oxide films has been examined by a number of authors [22,23,24,25,26]. The heterogeneous activities of aluminium [27,28,29,30] and iron [31] samples have also been investigated using SECM. Multimetallic materials have also been studied using the SECM and it was shown that specific metal-rich inclusions could be identified with pitting precursor sites [32]. However, to the best of our knowledge, SECM has not been used to analyse the surface of thermally-sprayed coatings. While process-inherent inclusions have been proposed as very important sites for local degradation of the coatings, spatially-resolved electrochemical data from the coatings is currently unavailable to verify this and SECM may become very useful in this regard.

In this contribution, the properties of Inconel 625 coatings on mild steel samples, prepared using HVOF thermal spraying, are examined using SECM. Using the feedback mode of SECM, the electrochemical behaviour of the coatings is compared with that of a wrought sample and a sample of Inconel 625 powder subjected to a simple sintering process. The three forms of Inconel 625 used have very different microstructures: the wrought material has no pores or spray-formed oxides, the sprayed coating has porosity and spray-formed oxides, and the sintered sample has porosity and minimal spray-formed oxides. By comparing the performance of these three Inconel 625 samples, the effect of different microstructural features can be determined. Feedback mode SECM was used to probe the local electrochemical activity of each material and regions of varying activity were identified on the thermally-sprayed material. Significantly, we show that the activity of the thermally-

sprayed Inconel 625 coating differed significantly from the bulk alloy. Therefore, these results show that SECM in the feedback mode may be used to rapidly analyse the local electrochemical activity of thermal-sprayed coatings of anti-corrosion coatings. Furthermore, we anticipate that high-resolution electrochemical activity data such as that shown here may have an impact on the development and optimisation of the HVOF process.

2. Experimental

2.1 Reagents and Apparatus

Wrought Inconel 625 was obtained as cold-rolled sheets from Special Metals Corporation (Hereford, UK). Gas-atomised Inconel 625 powder (Praxair 1265 F) with a nominal size of 20-53 μm was obtained from William Rowland Ltd. (Sheffield, UK). The average particle size was 39 μm. All chemicals were obtained at the highest grade available from Sigma-Aldrich and used as received. Electrochemical experiments were performed using a Model 910B scanning electrochemical microscope from CH Instruments Inc., Austin, Texas, USA. Aqueous solutions were prepared using Milli-Q (18.2 MΩ) deionized water.

2.2 Sample Preparation

Sintered Inconel 625 samples were produced by compacting the source powder using a single-acting uniaxial hydraulic press. The wall of the die was lubricated with acetone/lithium stearate (3:1) to reduce the frictional losses at the wall of the die and enable the compacted pellet to be removed easily from the die. 13 g of Inconel 625 powder was poured into the 22 mm diameter die, which was tapped to ensure an even distribution of the powder before

applying the compaction pressure (800 MPa at a force of 304 kN). The samples were then removed and sintered in a tube furnace in a flowing Ar environment (flow rate $\approx$ 200 cm^3 min^{-1}). The temperature was ramped from room temperature to the sintering temperature (1325 °C) at a rate of 20 °C min^{-1} and was held at 1325 °C for 60 minutes. The samples were then allowed to cool to room temperature in the inert atmosphere. The density of the sintered samples before and after sintering was obtained by measuring their mass and dimensions. The porosity was then determined by comparing the actual density of the sintered samples with that of the bulk alloy. For microstructural evaluation, transverse sections of the samples in the direction of the force were cut and polished to a roughness of approximately 1 μm. Optical microscopy and scanning electron microscopy were used to examine the morphology of the samples. Wrought samples were prepared for electron microscopy by immersing them in aqua regia at 40 °C for 10 s before rinsing thoroughly with water.

Prior to spraying, the steel coupons were degreased with industrial methylated spirit, followed by grit blasting using brown alumina (0.50 – 0.59mm diameter particles) as the blasting material. The grit blasting gun was held at 90° at a distance of about 7 cm above the surface of the sample and a pressure of 5.5 bar was applied. A MetJet-II liquid fuel HVOF system (Metallisation Limited, Dudley, UK) was used to deposit thermal-spray coatings on mild steel coupons with dimensions of 60 × 25 × 5 mm. The spray parameters were adjusted to produce reasonably dense coatings of approximately 350 μm thickness. The spray nozzle length was 100 mm and the spray distance was 350 mm. The oxygen and kerosene flow rates were 910 and 480 L min^{-1}, respectively, and the N_2 carrier gas flow rate was 4.6 L min^{-1}.

2.2 Surface Profilometry

Surface profile measurements were carried out using a Talysurf CLI 1000-3D system from Taylor Hobson Ltd., UK. The samples were mounted as standard metallographic samples and polished using 1 μm diamond paste on silica paper for the final polishing stage. All samples were polished in this way prior to SECM testing. During profilometry measurements, the samples were held in position using plasticine. A 2 μm radius diamond stylus was used to scan the surface of the sample. The workpiece was moved at a transverse speed of 500 μms^{-1}. Talymap 3D analysis software was used to determine the surface roughness. The average surface roughness, Ra, was 0.041 μm, 0.068 and 0.061 μm for the wrought sample, the sintered sample, and the Metjet HVOF thermally-sprayed sample, respectively.

2.3 Electrochemical Measurements

Scanning electrochemical microscopy was performed by placing a drop of the electrolyte solution containing the redox mediator onto the substrate and carefully inserting a saturated calomel electrode (SCE) and Pt wire counter electrode into the drop. The SECM tip approached the sample surface (through the electrolyte drop) from above. SECM tips were prepared by heat-sealing a platinum wire (5 μm radius, Goodfellow, UK) into soft glass tubing using a coil of nichrome resistance wire as the heat source, as described previously [33]. The Pt metal surface was exposed and polished using aqueous alumina slurries with successively smaller particle sizes from 1 μm to 0.05 μm. SECM tips with smaller radii (nominally 1.5 μm) were constructed by heat sealing a 25 μm Pt wire in a quartz capillary and pulling to a sharp point using a micropipette puller [33]. The platinum metal disk was exposed and the tip was sharpened using a micropipette beveller fitted with a diamond

polishing wheel, as described previously [34]. After polishing and sharpening, the SECM tips were examined using optical microscopy. The radii of the tips used in this study were approximately 5 μm or 1.5 μm with an *RG* value (= r_g/a, where r_g is the radius of the insulating glass sheath and *a* is the radius of the Pt wire) of approximately 2. The geometry of the SECM tip was confirmed prior to use using cyclic voltammetry and SECM feedback approach curve experiments (described later). The tip surfaces were gently polished using a 0.05 μm aqueous alumina slurry between measurements.

3.   Results and Discussion

3.1   *Microstructure of Wrought, Sintered and Thermal-Sprayed Inconel 625*

Inconel 625 is a Ni-Cr-Mo alloy, the nominal composition of which is shown in Table 1. The alloy is widely available in the form of sheets of the wrought material or as a powder and both source materials were used in this study. In the production of metallic components, it is often preferable to use sintered metals formed from powder sources due to the ease of processing compared to the difficult task of processing ingots of the solid. High-temperature sintering can also eliminate residual pores throughout the material and most of the sintering time is usually spent in attempting to eliminate large pores within the material [35]. In this study, we were interested in investigating the electrochemical properties of Inconel 625 as a function of microstructural features. Here, an incomplete sintering process was used to produce samples of Inconel 625 with a controlled level of porosity. Upon sintering the powdered Inconel 625 (average particle size 39 nm) at 1325 °C, large pores (20-30 μm diameter) were visible throughout the compacted material's surface while the majority of the surface was smooth because of the polishing technique used (Figure 1A). This surface differs significantly from

that of the etched wrought material, which showed no similarly-sized pores at the surface (Figure 1B). Our goal in this study was not to optimise the sintering process and the presence of these pores in the sintered material was actually useful here as they may give an insight into the local electrochemical activity of the pores when studied using SECM. Therefore, samples that showed such pores were used in the SECM analysis and this is described in a later section.

Thermally-sprayed coatings of Inconel 625 were formed from the powder source using a Metjet HVOF thermal spray technique. The sprayed material is a face-centred-cubic (fcc), solid-solution alloy, which can show some intermetallic phases and precipitated carbides depending on the treatment to which it is subjected [36]. The microstructure of the thermal-sprayed surface was significantly different to that observed in the wrought and sintered materials. Clear splat boundaries were observed at the interface between adjacent coating particles on the thermally-sprayed surface (Figure 1C). Pores can also be seen in these coatings and are due to the state of the particle when it impacts the substrate. The particles may arrive at the substrate surface in a fully molten, semi-molten, or fully-solid state depending on the extent of melting during transfer from the nozzle to the substrate. If the particles are not melted sufficiently, or are not travelling at high enough velocities, prior to impact with the substrate, they do not fill void spaces within the coating and pores form within the structure. Therefore, pore formation is typically associated with larger powder particles that do not melt or are not accelerated sufficiently prior to impact with the substrate. Preferential Cr oxidation before and upon impact can also cause the formation of Cr_2O_3-rich inclusions, resulting in fluctuating Cr content and a less than average Ni content [14,15]. These spray-formed oxides generally form within the fully melted zones between adjacent splat boundaries [37]. The presence of such pores and inclusions is undesirable as it has been

proposed that such features may contribute to corrosion effects in the sprayed coatings [14,15].

3.2 Scanning Electrochemical Microscopy

SECM is a high-resolution scanning probe technique that employs the faradaic reaction occurring between an ultramicroelectrode (UME) and a substrate surface as the analytical signal [21]. When a redox species in solution is oxidized or reduced at a disk-shaped UME, the steady-state current that flows when the tip is positioned far from a substrate, $i_{T,\infty}$, is given by equation 1:

$$i_{T,\infty} = 4.43nFDCa \qquad\qquad (1)$$

where n is the number of electrons transferred during the redox reaction, F is the Faraday constant, D is the diffusion coefficient of the redox species, C is the bulk solution concentration of the redox species and a is the radius of the UME. The constant 4.43 appears in equation 1 due to the small RG value of the electrodes used here, which causes an increase in the availability of reactant diffusing from behind the plane of the electrode (i.e. a current increase of approximately 10 % over that for an electrode with large RG) [38]. When the UME (SECM tip) is positioned close to a substrate surface, diffusion of the species to the tip can be affected in a number of ways. In the positive feedback mode regeneration of the redox species can occur at conducting substrates leading to enhanced flux to the tip and an increase in the tip current ($i_T > i_{T,\infty}$). Conversely, in the negative feedback mode, regeneration of the redox species at the substrate cannot occur and diffusion of the redox species to the tip is blocked resulting in a decrease in the tip current ($i_T < i_{ss}$). Therefore, the positive and

11

negative feedback modes of SECM can be used to differentiate between conducting and insulating regions on a topographically-smooth surface. Finally, if the redox species is regenerated at the substrate at a finite rate, i_T will be intermediate between each extreme and surface kinetic information may be obtained.

In this study, SECM in the feedback mode was used to examine the local electrochemical activity of the thermally-sprayed coatings, which was compared with that of the wrought and sintered material. Ferrocenemethanol (FcOH) was used as the redox mediator because, as has been shown previously, it undergoes reversible oxidation at Pt UME surfaces [39]. Figure 2 shows a typical steady-state cyclic voltammogram recorded at a 5 μm radius platinum UME in a solution of FcOH. The steady-state current, $i_{T,\infty}$, was 1.5 nA, which agreed closely with that expected for a 5 μm radius UME in a 1 mM solution of FcOH, and the half-wave potential of FcOH was 0.190 V vs SCE. Using optical microscopy, the radius of the Pt disk was estimated to be 5 μm, which agreed with the nominal radius of the Pt microwire. Using careful polishing and sharpening, it was possible to reduce the *RG* value of the SECM tip to approximately 2 (based on optical microscopy) and SECM approach curve experiments were then used to determine the geometry of the SECM tip. Figure 3 shows normalised positive and negative feedback approach curves obtained in a solution of FcOH as the tip approached conducting (platinum disk) and insulating (PTFE) substrates. Theoretical feedback approach curves were generated using equations 2 and 3 for pure positive and negative feedback, respectively.

$$i_T(L) = k_1 + k_2 / L + k_3 \exp(k_4 / L) \qquad (2)$$

$$i_T(L) = 1/[k_1 + k_2 / L + k_3 \exp(k_4 / L)] \qquad (3)$$

where $i_T(L)$ is the normalized tip current at distance L from the substrate. L is the normalized distance between the tip and the substrate, d/a, where d is the tip-substrate distance and a is the tip radius. The constants in equations 2 and 3 have been calculated for SECM tips with various RG values and the theoretical curves in Figure 3 were generated for tips with $RG = 2$ [21]. Clearly, good agreement between the experimental and theoretical approach curves was observed in each case, indicating that the radius and RG value estimated using optical microscopy were accurate. Deviations of the experimental curves from the theoretical curves were observed at $L = 0.06$ ($i_T(L) = 0.15$) in the negative feedback curve due to crashes of the tips into the substrate. However, occasional crashes such as these did not affect the geometry of the tip to any significant extent. The ability to approach to such small distances $L < 0.1$ was due to the careful sharpening of the tip to reduce the RG value and is essential when attempting to examine the tip geometry. Furthermore, this permits a wide range of tip-substrate distances to be used during SECM imaging in the feedback mode.

3.4 Scanning Electrochemical Microscopy at Wrought and Sintered Inconel 625 Surfaces

The electrochemical properties of wrought and sintered Inconel 625 were studied using SECM to obtain insights into the electrochemical activity of this material prior to thermal spraying. Figure 4A shows an approach curve obtained using a 1.5 μm radius Pt SECM tip at a random location on the wrought sample surface. Also shown is the theoretical response generated for a 1.5 μm tip with $RG = 2$ approaching a purely insulating substrate. Clearly, excellent agreement is observed between the experimental and theoretical approach curves indicating that the surface of the wrought material behaves as a pure insulator. The presence of the protective oxide layer formed naturally at the Ni-Cr-Mo alloy is the reason for the observed insulating behaviour and the anti-corrosion properties of this material. Upon

scanning the SECM tip in the *x-y* plane, while positioned sufficiently close to the substrate for negative feedback at the tip, an almost featureless SECM image was obtained (Figure 4B), indicating no obvious regions of high electrochemical activity exist on the surface. The slight increase in the tip current as the tip reached the bottom of the area shown in Figure 4B was due to a slight tilt in the substrate and this was verified by recording negative feedback approach curves at a number of points across the substrate surface, all of which showed purely insulating behaviour.

Figure 5A and 5B show a feedback approach curve and a feedback-mode SECM image recorded using a 5 μm tip and a sample of sintered Inconel 625 as substrate. The point on the substrate at which the approach curve shown in Figure 5A was recorded is indicated by a black circle in the image shown in Figure 5B. Also shown in Figure 5A is the theoretical approach curve generated for a 5 μm tip with $RG = 2$ approaching a purely insulating substrate. Again, excellent agreement between the experimental and theoretical curves was observed at this location on the substrate surface, indicating that the Inconel 625 surface behaves as a pure insulator, even after sintering at over 1000 °C. Regions of higher tip current can also be observed in Figure 5B, indicated in the image by yellow or brown features. These regions are approximately disk-shaped and correspond to pores in the surface, which can be verified by comparing the SECM image shown in Figure 5B with the SEM image of the sintered sample surface shown in Figure 1A. The increase in the tip current at these locations can be due to either topographic effects (a decrease in the negative feedback as the tip passes over the pore) or an increase in the electrochemical activity in the region of the pore. The cause of this higher current was examined by positioning the tip above the pore shown at the bottom of the image in Figure 5B and recording an approach curve as the tip approached the surface. This is shown in Figure 6, where the experimental curve is compared to the theoretical positive and negative feedback approach curves. As the tip approached the

surface in the vicinity of the pore, a slight increase in the tip current was observed. At small L values, the tip current was higher than that expected for a pure insulator and smaller than that expected for a pure conducting substrate, indicating sluggish regeneration of the redox mediator at the substrate surface near the pore. At $L \approx 0.4$, i_T reached a steady value, which did not increase as the tip was moved closer to the substrate. This response is most likely due to a crash of the tip with the walls of the pore, resulting in hindered movement of the tip and the resulting displacement-independent i_T. Nonetheless, it is clear from Figure 6 that the local electrochemical activity of the sintered material near the pore differs significantly from that observed at the majority of the surface (Figure 5A). We are currently exploring the source of this local electrochemical activity and, as we have shown here, SECM may become very useful for examining the local electrochemical activity of sintered alloys with varying degrees of porosity.

3.5   Scanning Electrochemical Microscopy of Thermal-Sprayed Inconel 625 Coatings

Figure 7A and 7B show feedback approach curves and a feedback-mode SECM image obtained using a 5 μm radius tip and a substrate consisting of a stainless steel coupon coated with a 300 μm thick thermal-sprayed coating of Inconel 625. The locations at which the two experimental approach curves were recorded are indicated in Figure 7B by arrows. Also shown in Figure 7A is the theoretical negative feedback approach curve generated for a 5 μm radius tip with $RG = 2$. Clearly, neither experimental approach curve fit the theoretical curve well. While both experimental curves showed some insulating behaviour ($i_T < i_{T,\infty}$ at $L < 1$), slow regeneration of the redox mediator at the substrate surface caused deviations from the theoretical response. The approach curve recorded at a region that showed a higher current in the SECM image (an "active" spot) showed slightly more positive feedback than the curve

recorded at a region of low current (an "inactive" spot). This indicates that the variation observed in SECM imaging of the coating surface was due to increased local electrochemical activity at various locations on the surface. Significantly, the dimensions of the features in Figure 7B (20-50 μm) correspond quite well with the dimensions of the splats observed by SEM analysis of the sprayed coatings. The clear differences in the approach curves obtained at the sprayed surface and those recorded at the wrought and sintered surfaces clearly indicate that the increased electrochemical activity of the material is introduced during the spraying process. The origin of the high electrochemical activity of the thermal-sprayed sample cannot be identified using our analysis. However, it is likely that preferential Cr oxidation occurs during the spray process, which causes the formation of Cr_2O_3-rich domains on the surface [15]. It is possible that the resultant oxide layer at these regions is very thin or absent, resulting in increased electron transfer across the substrate/electrolyte interface and we are currently investigating this further.

It should be emphasised that the regions of high and low electrochemical activity observed using SECM imaging corresponded to varying local electrochemical activities on the surface, as opposed to any topographic effects. The surface roughness was examined using surface profilometry (described above) and, from this analysis, any features present on the coating surface were expected to be smaller than those detectable using a 5 μm radius SECM tip. Furthermore, during approach curves recorded at regions of varying conductivity on the surface, such as those shown in Figure 7A, the insulating material of the tip tended to touch the substrate surface at approximately the same tip displacement, indicating that sample tilt and topographical effects were negligible during these measurements. Considering this, and the differences observed in the approach curves shown at regions of varying activity, we can conclude that the features in the SECM images of the thermal-sprayed coatings are solely due to heterogeneity of the surface in terms of electrochemical activity.

The electrochemical activity of these coatings was further investigated by recording feedback approach curves at a range of substrate potentials, E_S. Figure 8 shows approach curves recorded using a 5 μm radius tip as the tip approached a stainless steel coupon coated with a thermal-sprayed coating of Inconel 625. Also shown is the theoretical curve generated for a 5 μm tip with $RG = 2$ approaching a purely insulating substrate. In this experiment, the tip approached an "inactive" spot on the surface, similar to that shown in Figure 7B (i.e. a region of low activity). The experimental E_S values used were the open circuit potential (OCP), -0.1 V vs SCE and -0.2 V vs SCE. At OCP, the experimental curve deviated slightly from that of the theoretical curve, as is also shown in Figure 7A. However, at -0.1 V and -0.2 V vs SCE, respectively, the extent of positive feedback observed in the approach curves increased substantially, indicating faster regeneration of the redox mediator at negative substrate potentials. This observation further supports our conclusion that regions of high electrochemical activity on thermal sprayed coatings of Inconel 625 identified using the SECM correspond to regions of enhanced electron transfer across the substrate/electrolyte interface, the rate of which can be altered by systematically altering the driving force for electron transfer, E_S. Therefore, it appears that the current thermal spray process does have a detrimental effect on the electrochemical properties of this alloy. Furthermore, our identification of regions of high and low electrochemical activity on the thermally-sprayed surface confirm that microstructural properties may indeed be the cause of corrosive failure of devices fabricated using this material. We are currently using SECM as an analytical tool for the optimisation of the thermal spray process and anticipate that elimination of microstructural heterogeneity may result in significant improvements in the performance of this material. Furthermore, we are in the process of simulating feedback approach curve experiments at these thermally-sprayed surfaces under various conditions. These experiments may yield new insights into the mechanism of charge transfer at these surfaces, as well as

quantitative data that we can use in the optimisation of the process and this will be described in a future contribution.

4.0   Conclusions

The electrochemical activity of various forms of Inconel 625 was studied using scanning electrochemical microscopy. Based on approach curve data, it was shown that Inconel 625 in its wrought state behaves as a pure insulator with no obvious regions of high electrochemical activity visible on the surface. Upon sintering the powdered source material, the surface of the alloy remained insulating while large pores appeared throughout the surface and these pores were also identified as regions of high electrochemical activity. However, significant differences were observed at thin coatings of the alloy formed at mild steel substrates. SECM imaging revealed that regions of varying conductivity were formed during spraying and feedback approach curves showed that the material no longer behaved as a pure insulator. Therefore, it appears that the thermal-spraying process has a detrimental effect on the electrochemical properties of Inconel 625 and that the local electrochemical activity of the surface is quite heterogeneous, which is most likely related to the microstructural features introduced during thermal spraying. Thus, we have shown here for the first time that SECM can rapidly provide very useful information, with high spatial resolution, regarding the quality and local electrochemical activity of thermally-sprayed anti-corrosion coatings.

Acknowledgements

TABLE 1: Nominal composition of Inconel 625 powder

Element	Ni	Cr	Mo	Nb	Si	Co	Mn
wt %	65.1	22.0	9.0	3.4	0.2	0.2	0.1

FIGURE LEGENDS

Figure 1.   Scanning electron micrographs of (A) sintered Inconel 625, (B) wrought Inconel 625 after chemical etching with warm (40 °C) aqua regia for 10 s, and (C) a HVOF thermal-sprayed coating of Inconel 625 on a mild steel substrate.

Figure 2.   Steady-state voltammogram obtained at a 5 μm radius Pt SECM in 1 mM FcOH in 0.1 M Na_2SO_4. The scan rate was 5 mV s^{-1} and the potential was scanned between 0.0 and 0.5 V vs SCE. The initial potential was 0.0 V vs SCE.

Figure 3.   Negative (lower) and positive (upper) feedback approach curves obtained during the oxidation of FcOH as the SECM tip approach a Teflon substrate and a 2 mm Pt disk substrate, respectively. In each case, the SECM tip was a 5 μm radius Pt disk, the solution was 1 mM FcOH in 0.1 M Na_2SO_4 and the tip was held at 0.5 V vs SCE. The tip approach rate was 1 μm s^{-1} in each case. Experimental curves are shown by the solid lines and theoretical curves generated for a 5 μm tip with $RG = 2$ are shown by the open circles.

Figure 4.   (A) Negative feedback approach curve obtained for the oxidation of FcOH as the SECM tip approach the surface of wrought Inconel 625. The SECM tip was a 1.5 μm radius Pt disk, the approach rate was 0.25 μm s^{-1} and the solution was 1 mM FcOH/0.1 M Na_2SO_4. The experimental curve is shown by the solid line and the theoretical curve for a 1.5 μm tip with $RG = 2$ is shown by the open circles. (B) SECM image recorded by recording i_T while scanning the tip across the surface in the *x-y* plane at 60 μm s^{-1}. The experimental conditions were as described in (A) and the tip-substrate separation, L, was 2 μm.

Figure 5. (A) Negative feedback approach curve obtained for the oxidation of FcOH as the SECM tip approach the surface of sintered Inconel 625. The SECM tip was a 5 μm radius Pt disk, the approach rate was 0.25 μm s^{-1} and the solution was 1 mM FcOH/0.1 M Na$_2$SO$_4$. The experimental curve is shown by the solid line and was recorded at the position shown by the arrow. The theoretical curve for a 5 μm tip with $RG = 2$ is shown by the open circles. (B) SECM image recorded by recording i_T while scanning the tip (at a distance of 10 μm) across the surface in the x-y plane at 60 μm s^{-1}. The experimental conditions were as described in (A).

Figure 6. Feedback approach curve obtained using a 5 μm Pt SECM tip as the tip approached the pore shown at the bottom of Figure 5A. Experimental conditions are as described for Figure 5. The open circles show the theoretical positive (upper) and negative (lower) feedback approach curves for a 5 μm tip with $RG = 2$.

Figure 7. (A) Feedback approach curves obtained for the oxidation of FcOH as a 5 μm radius Pt SECM tip approach the surface of sintered Inconel 625. The approach rate was 0.25 μm s^{-1} and the solution was 1 mM FcOH/0.1 M Na$_2$SO$_4$. The experimental curves are shown by the solid lines and were recorded at the positions indicated by the arrows. The theoretical curve for a 5 μm tip with $RG = 2$ is shown by the open circles. (B) SECM image recorded by recording i_T while scanning the tip (at a distance of 10 μm) across the surface in the x-y plane at 60 μm s^{-1}. The experimental conditions were as described in (A).

Figure 8. Approach curves obtained for the oxidation of FcOH as a 5 μm radius Pt SECM tip approach the surface of sintered Inconel 625. The approach rate was 0.25 μm s^{-1}

and the solution was 1 mM FcOH/0.1 M Na_2SO_4. The experimental approach curves (solid lines) were recorded at open circuit potential (lower solid line), -0.1 V vs SCE (middle solid line) and -0.2 V vs SCE (upper solid line). The theoretical positive (upper) and negative (lower) approach curves for a 5 μm tip with $RG = 2$ are shown by the open circles.

FIGURE 1

FIGURE 2

200 nA

0.4   0.2   0

E / V vs SCE
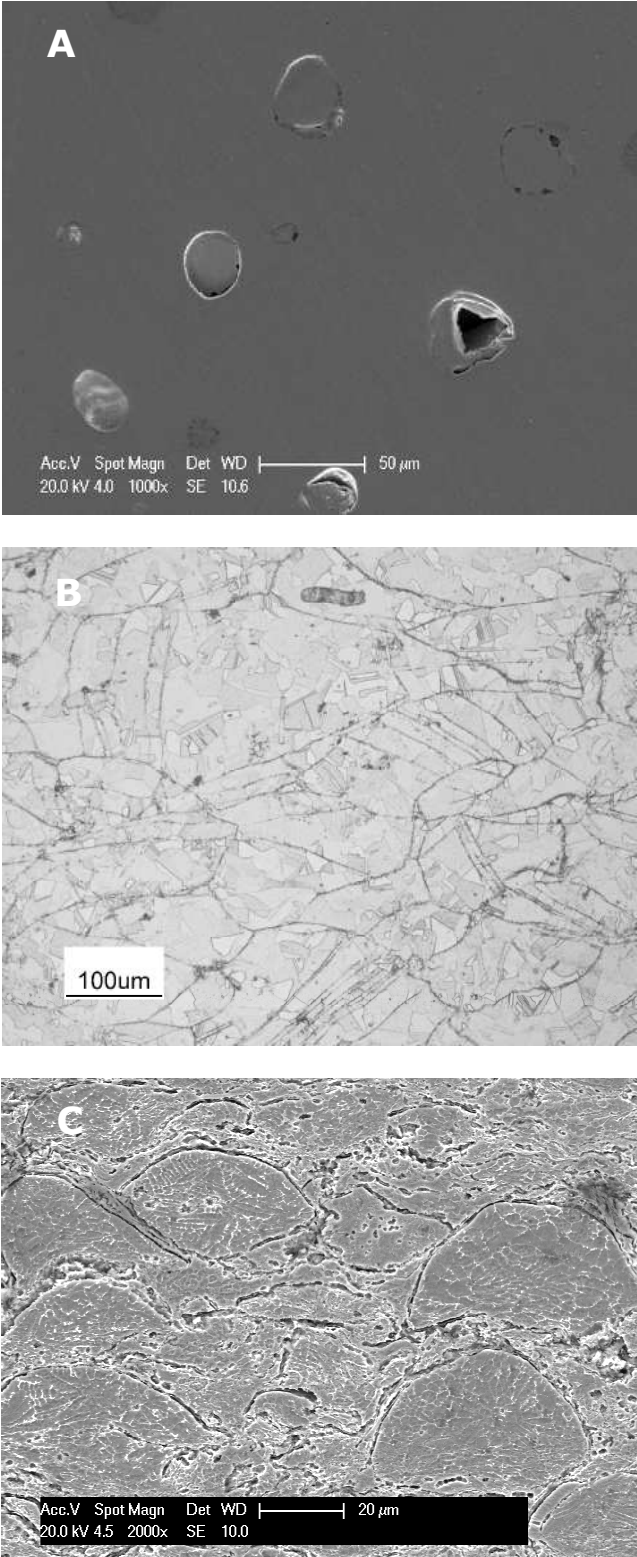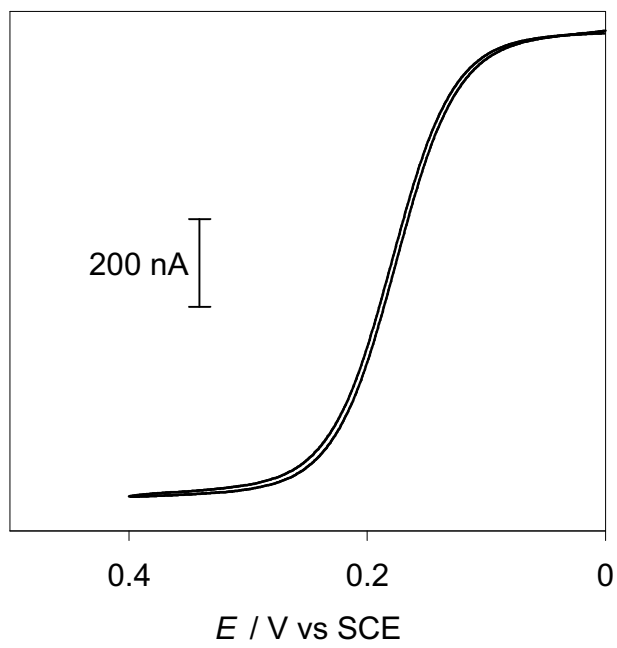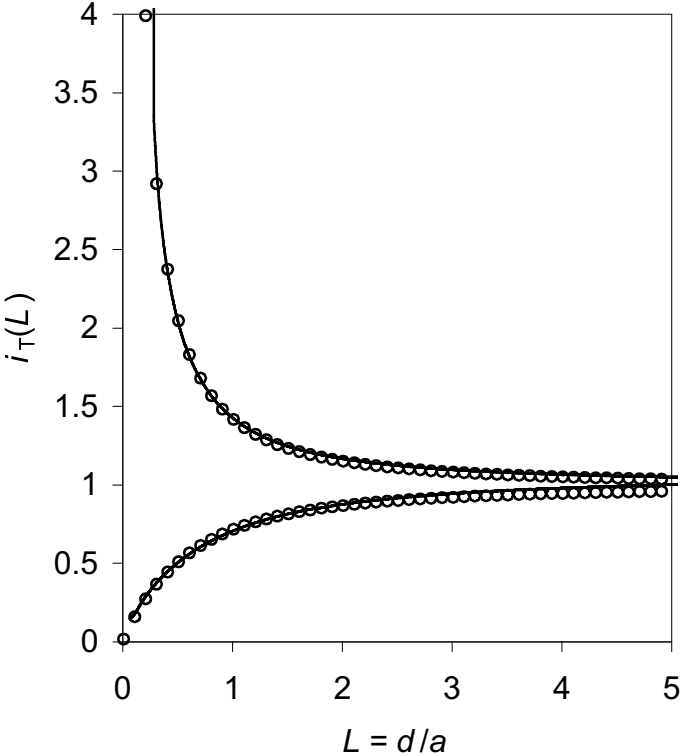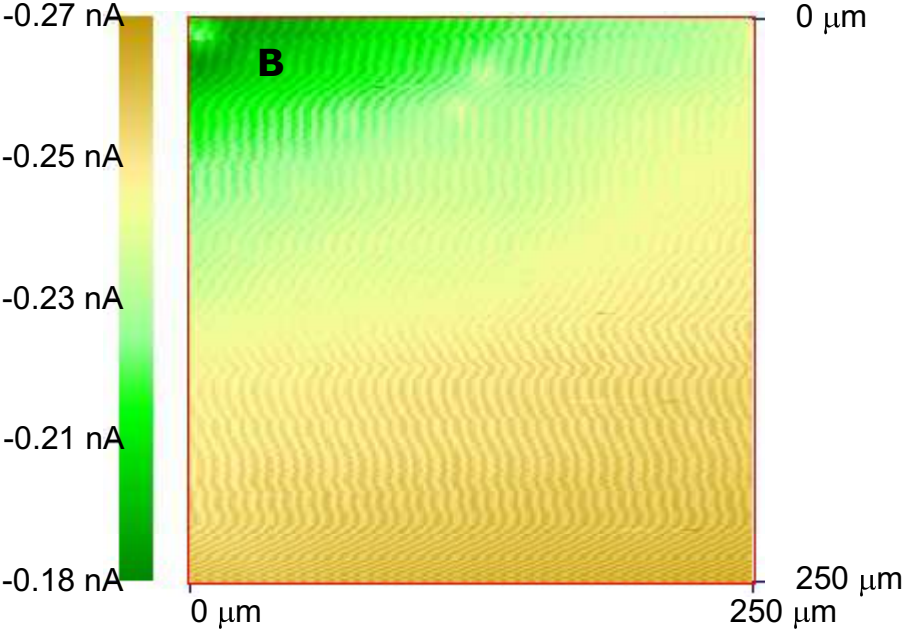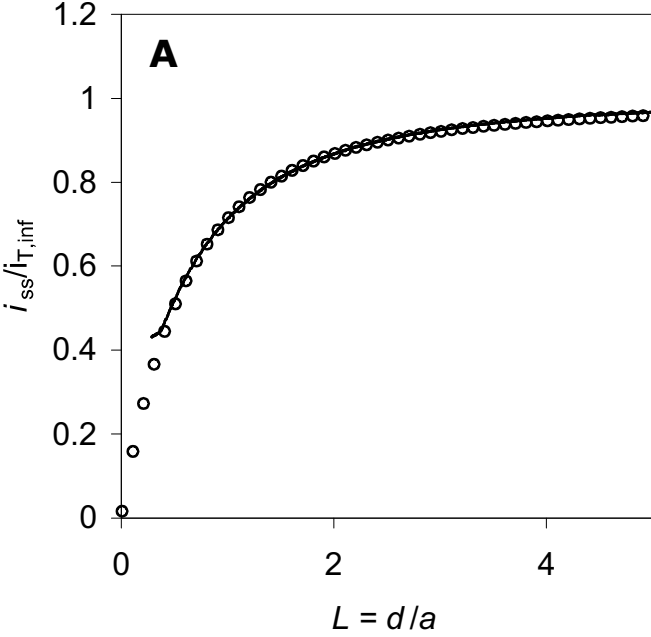
FIGURE 3

FIGURE 4

FIGURE 5
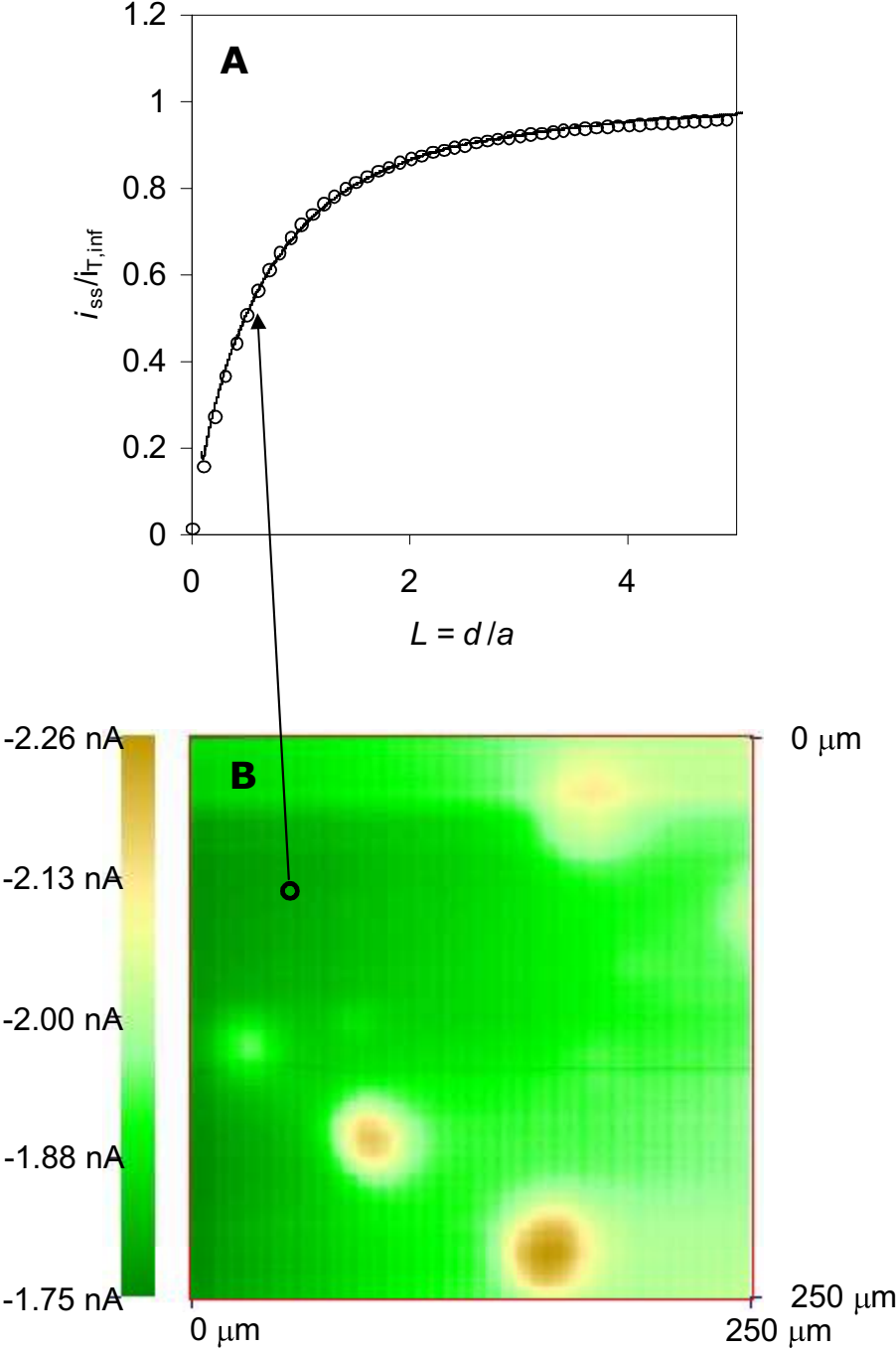
FIGURE 6
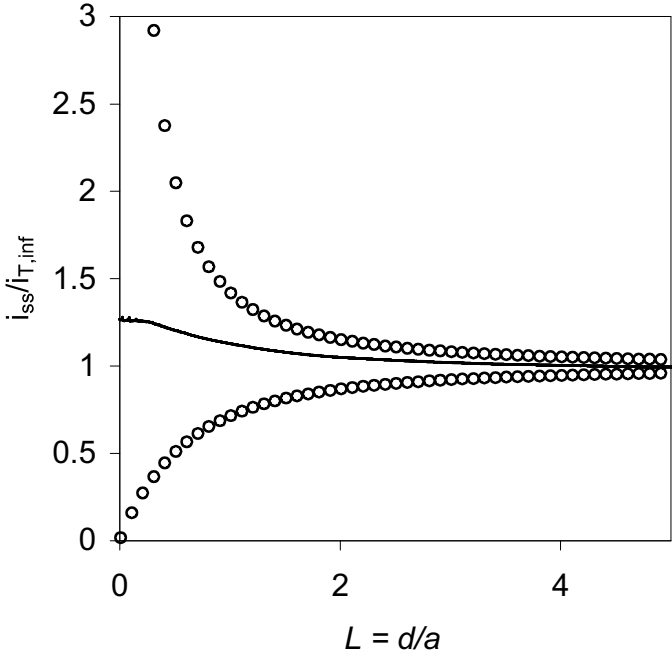
FIGURE 7
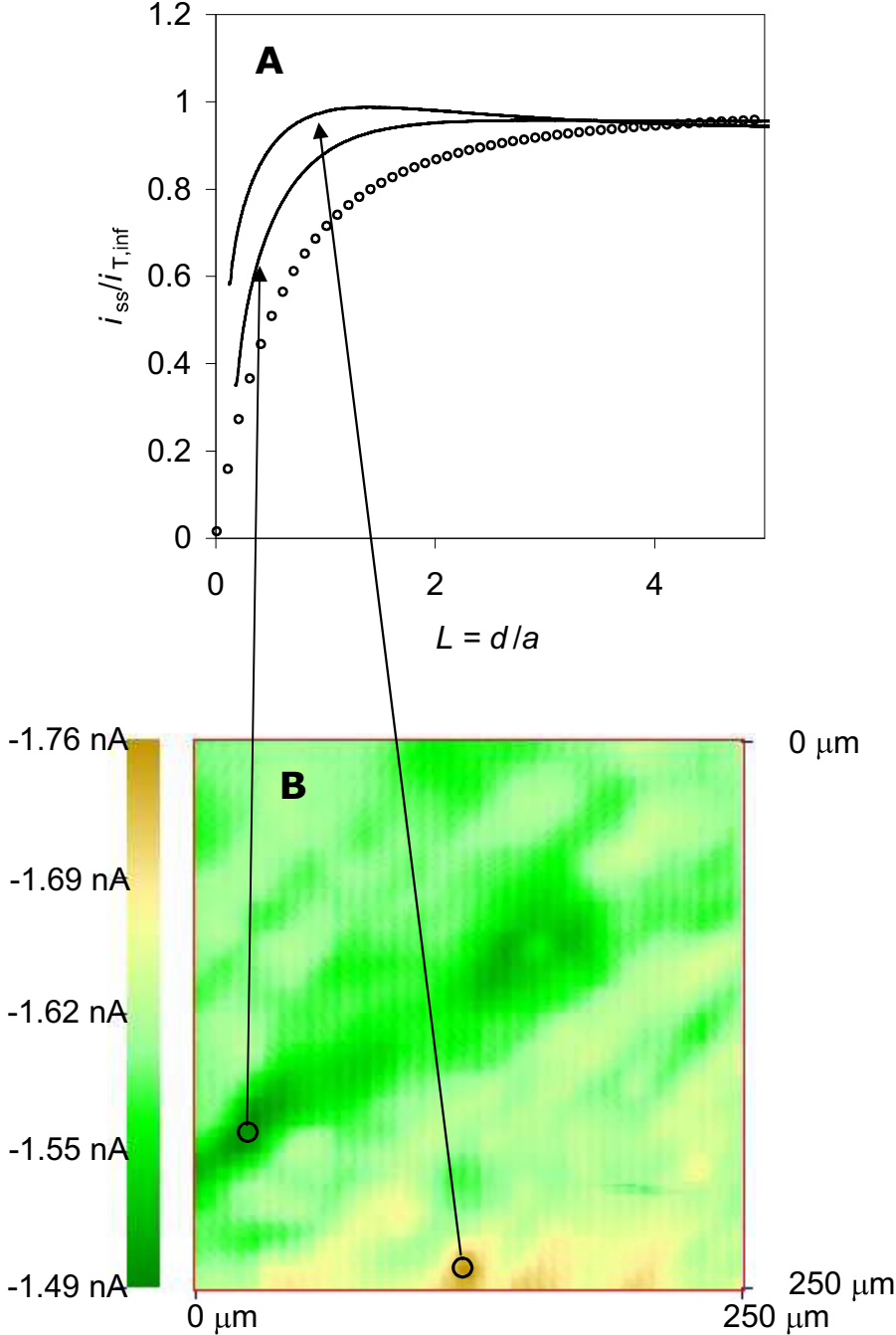
FIGURE 8
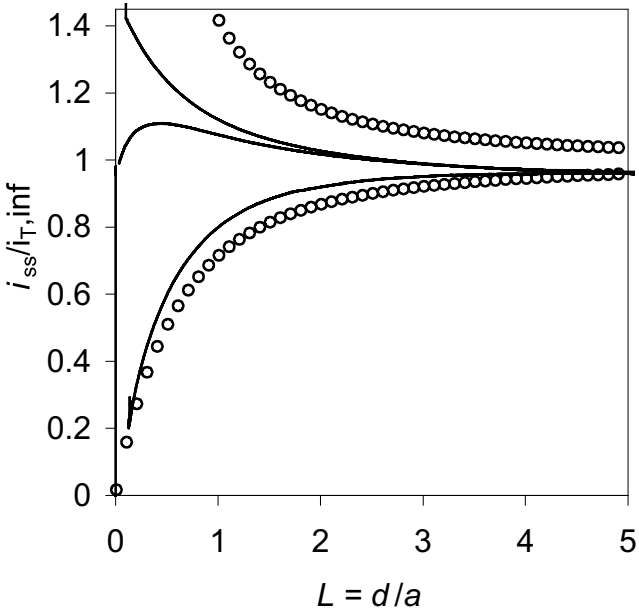
References

[1] M. L. Berndt, C. C. Berndt, Thermally Sprayed Coatings, in: S. D. Cramer, B. S. Covino Jr. (Eds.), ASM Handbook Vol. 13 Corrosion: Fundamentals, Testing and Protection; ASM International, USA, 2003.

[2] D. W. Parker, G. L. Kutner, Adv. Mater. Processes 139 (1991) 68.

[3] D. W. Parker, G. L. Kutner, Adv. Mater. Processes 146 (1994) 31.

[4] A. Ibrahim, R. S. Lima, C. C. Berndt, B. R. Marple, Surf. Coat. Technol. 201 (2007) 7589.

[5] R. S. Lima, K. A. Khor, H. Li, P. Cheang, B. R. Marple, Mat. Sci. Eng. A 396 (2005) 181.

[6] N. Espallargas, J. Berget, J. M. Guilemany, A. V. Benedetti, P. H. Suegama, Surf. Coat. Technol. 202 (2008) 1405.

[7] L. -M. Berger, S. Saaro, T. Naumann, M. Kasparova, F. Zahalka, J. Thermal Spray Techn. 17 (2008) 395.

[8] C. J. Villalobos-Gutiérrez, G. E. Gedler-Chacón, J. G. La Barbera-Sosa, A. Piñeiro, M. H. Staia, J. Lesage, D. Chicot, G. Mesmacque, E. S. Puchi-Cabrera, Surf. Coat. Technol. 202 (2008) 4572.

[9] M. Li, D. Shi, P. D. Christofides, Ind. Eng. Chem. Res. 43 (2004) 3632.

[10] E. Dongmo, M. Wenzelburger, R. Gadow, Surf. Coat. Technol. 202 (2008) 4470.

[11] M. Hasan, J. Stokes, L. Looney, M. S. J. Hashmi., Surf. Coat. Technol. 202 (2008) 3215.

[12] E. Turunen, T. Varis, T. E. Gustafsson, J, Keskinen, T. Fält, S.-K. Hannula, Surf. Coat. Technol. 200 (2006) 4987.

[13] D. Zhang, S. J. Harris, D. G. McCartney, Mat. Sci. Eng. A 344 (2003) 45.

[14] N. Ahmed, K. T. Voisey, D. G. McCartney, I.R. Pashby, Proc. Eurocorr 2007, The European Corrosion Conference, Freiburg im Breisgau, Germany, Sept. 2007.

[15] N. Ahmed, K. T. Voisey, D. G. McCartney, I. R. Pashby, In Proc. 4th International WLT-Conference on Lasers in Manufacturing 2007, Munich, June 2007, 401-406.

[16] R. Baccino, F. Moret, F. Pellegrin, D. Guichard, G. Raisson, Mater. Design 21 (2000) 345.

[17] L. Sexton, S. Lavin, G. Byrne, A. Kennedy, J. Mater. Process Technol. 122 (2002) 63.

[18] A. C. Llyod, J. J. Noél, S. McIntyre, D. W. Shoesmith, Electrochim. Acta. 49 (2004) 3015.

[19] Z. Liu, J. Cabrero, S. Niang, Z. Y. Al-Taha, Surf. Coat. Technol. 210 (2007) 7149.

[20] J. Suutala, J. Tuominen, P. Vuoristo, Surf. Coat. Technol. 201 (2006) 1981.

[21] A. J. Bard, M. V. Mirkin (Eds.), Scanning Electrochemical Microscopy, Marcel Dekker, New York, 2001.

[22] N. Casillas, S. J. Charlebois, W. H. Smyrl, H. S. White, J. Electrochem. Soc. 140 (1993) L142.

[23] R. Zhu, C. Nowierski, Z. Ding, J. J. Noël, D. W. Shoesmith, Chem. Mater. 19 (2007) 2533.

[24] S. B. Basame, H. S. White, J. Phys. Chem. 99 (1995) 16430.

[25] N. Casillas, S. Charlebois, W. H. Smyrl, H. S. White, J. Electrochem. Soc. 141 (1994) 6363

[26] R. K. Zhu, Z. Q. Qin, J. J. Noel, D. W. Shoesmith, Anal. Chem. 80 (2008) 1437.

[27] D. O. Wipf, Colloid Surface A 93 (1994) 251.

[28] M. B. Jensen, A. Guerard, D. E. Tallman, G. P. Bierwagen, J. Electrochem. Soc. 155 (2008) C324.

[29] J. C. Seegmiller, D. A. Buttry, J. Electrochem. Soc. 150 (2003) B413.

[30] A.M. Simões, D. Battocchi, D.E. Tallman, G.P. Bierwagen, Corr. Sci. 49 (2007) 3838.

[31] C. Gabrielli, S. Joiret, M. Keddam, H. Perrot, N. Portail, P. Rousseau, V. Vivier, J. Electrochem. Soc. 153 (2006) B68.

[32] M. A. Malik, P. J. Kulesza, Anal. Chem. 79 (2007) 3996.

[33] F.R.F. Fan, J. Fernández, B. Liu, J. Mauzeroll, C. G. Zoski, in: C. G. Zoski (Ed.), Handbook of Electrochemistry, Elsevier, Amsterdam, 2007, Ch. 6.3.

[34] A. W. Taylor, F. Qiu, J. Hu, P. Licence, D. A. Walsh, J. Phys. Chem. B 112 (2008) 13292.

[35] J. Pan, H. N. Ch'ng, A. C. F. Cocks, Mech. Mater. 37 (2005) 705.

[36] E.A. Loria (Ed.), Superalloys 718, 625 and Various Derivatives, The Minerals, Metals and Materials Society, Warrendale, PA, 1991.

[37] H. Edris, D.G. McCartney, A.J. Sturgeon, J. Mater. Sci. 32 (1997) 863.

[38] Amphlett, J. L.; Denault, G., J. Phys. Chem. B 102 (1998) 9946.

[39] W. Miao, Z. Ding, A. J. Bard, J. Phys. Chem. B 106 (2002) 1392.